Analytical Solution of the Switching Trap Model for Negative Bias Temperature Stress

B. Bindu[†], W. Goes[*], Ben Kaczer[°], and Tibor Grasser[*]

[*] CDL for TCAD at the [†]Institute for Microelectronics, TU Vienna, Vienna, Austria
[°] IMEC, 3001 Leuven, Belgium

***Abstract*—Negative bias temperature instability (NBTI) is a serious reliability issue for p-channel MOSFETs when stressed with negative gate voltages at high temperatures. There is not any analytical models of NBTI reported so far, which considers the dynamics of NBTI that are commonly observed in experimental data obtained from fast measurement techniques. An analytical model for NBTI is urgently required for circuit simulation purposes. In this paper, we present an analytical solution of switching trap model, which explains the dynamics of negative bias temperature stress.**

I. Introduction

The traditionally employed reaction-diffusion theory for modeling the negative bias temperature instability is based on a diffusion-limited creation and annealing of interface states [1, 2]. Recent reports have clearly demonstrated the failure of this model to capture the dynamic properties of the phenomenon, including the logarithmic recovery, AC vs. DC stress, the duty-factor dependence, and the strong gate voltage sensitivity during recovery [3–6]. Even though the physical mechanisms behind NBTI are still controversial, It is recently reported that there are two mechanisms mainly contributing to NBTI which are (i) trapping of holes into the oxide and (ii) creation of interface states [7–10]. The former is responsible for the recoverable component and latter for the permanent component of NBTI.

We have recently suggested a model that can succesfully explain the experimentally observed features [8]. The model assumes that in stage one individual defect precursors (oxygen vacancies) can capture holes, which in stage two favors the creation of interface states. Due to the amorphous nature of the oxide, the defects are assumed to exist with a wide distribution of properties, most importantly the multiphonon barriers, the energetic levels of the precursor and the created defect. Lacking more detailed information, uniform distributions of these barriers and levels have been assumed so far, consistent with previous reports on oxide defects [11]. While each single defect is described by only one set of coupled rate equations, the overall (measurable) degradation is obtained by averaging the responses of a large number of such individual defects. So far, only numerical solutions of the resulting equation system have been given. Unfortunately, the impact of the individual model parameters on the model behavior is obscured by the numerical solution procedure. In order to better understand their impact and also to provide reliability engineers with an tool-box that is intuitive to use, an analytic solution of the model is urgently needed. This is a formidable task and first results for the hole capture component (stage one) will be presented in this paper. Section 1 explains the analytical solution of the recoverable charge trapping component of NBTI and a simplified solution of the model is presented in Section 2. The validation of the model by comparing with experimental data is given in Section 3. The conclusions are drawn in Section 4.

II. Analytical Solution

Fig. 1 shows the Harry-Diamond-Labs (HDL) switching trap model [9] that is used to model the recoverable charge component of NBTI (stage one of [8]). Upon application of stress, the Si-Si bond of the precursor breaks and a hole is trapped into an oxygen vacancy at the silicon-oxide interface which creates a positively charged E'_γ center (state 2 in Fig. 1). The hole is captured via a field-assisted lattice relaxation multiphonon emission (LRME) mechanism [12, 13]. The positively charged E'_γ center in state 2 can be neutralized by emission of a hole (capture of electron). This is represented as transition from state 2 to state 3 and the defect is neutral at state 3. Being in state 3, either a hole can be captured again (a transition from state 3 to state 2) or the structure can relax back to its equilibrium state (transition from state 3 to state 1). Thus, the defect is positively charged only when it is in state 2.

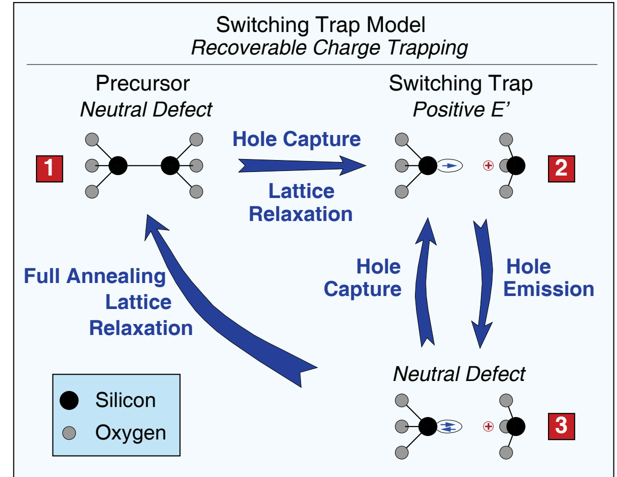

Fig. 1. The Harry-Diamond-Labs (HDL) switching trap model [9] used previously to model the recoverable charge trapping component of NBTI (stage one) [8]. It assumes that a defect is created from the precursor state 1 by capturing a hole via a field-assisted lattice relaxation multiphonon emission (LRME) mechanism [12, 13]. Once the defect is created, its charge state quickly follows the Fermi-level, being positive in state 2 and neutral in state 3. Full annealing of the defect is possible from the neutral state 3 only.

The rate equations describing stage one (cf. Fig. 1) read

$$\dot{f}_1 = -\, f_1 k_{12} + (1 - f_1 - f_2) k_{31}, \tag{1}$$

$$\dot{f}_2 = +\, f_1 k_{12} - f_2 k_{23} + (1 - f_1 - f_2) k_{32}. \tag{2}$$

where the hole capture and emission rates are calculated using similar procedure reported in [8] as

$$k_{12} = p\, v_p^{\mathrm{th}}\, \sigma_p\, \mathrm{e}^{-\beta(\Delta E_{\mathrm{B}} + E_{\mathrm{VT}}) + F^2/F_{\mathrm{c}}^2},$$

$$k_{23} = p\, v_p^{\mathrm{th}}\, \sigma_p\, \mathrm{e}^{-\beta E_{\mathrm{T'F}}},$$

$$k_{32} = p\, v_p^{\mathrm{th}}\, \sigma_p \qquad \text{and}$$

$$k_{31} = \nu\, \mathrm{e}^{-\beta \Delta E_{\mathrm{A}}}.$$

 978-1-4244-3922-5/09/$25.00 ©2009 IEEE

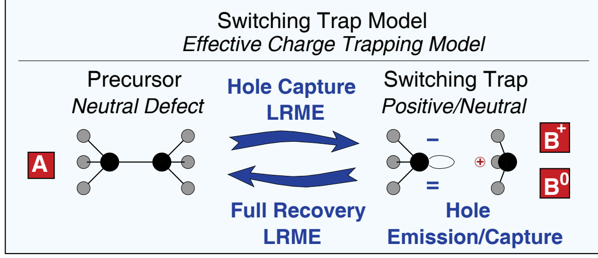

Fig. 2. Under the assumption that the transition rates between states 2 and 3, k_{23} and k_{32}, are much larger than k_{12} and k_{31}, effective rates $k_{\mathrm{AB}} \approx k_{12}$ and $k_{\mathrm{BA}} \approx k_{31}/(1+k_{32}/k_{23})$ can be defined. The factor $1/(1+k_{32}/k_{23})$ gives the occupancy of state B according to Fermi-Dirac statistics and considerably increases the charge detrapping time when the defect is positively charged.

Here, p is the hole concentrations in the channel, v_p^{th} the thermal velocity, σ_p the capture cross section, E_{F} the Fermi-level in the channel, E_{V} the valence band, E_T the trap level, ΔE_{A} and ΔE_{B} the multiphonon emission (MPE) barriers, F_{c} the reference field for the multiphonon-field-assisted tunneling mechanism (MPFAT) and $\beta = 1/\mathrm{k_B}T$.

The probability of being in state i is denoted by f_i while the transition rates from state i to j are given by k_{ij} [8]. Macroscopically observable quantities are obtained by summing the individual responses

$$\langle m \rangle = N \int \mathrm{d}\mathbf{X}\; m\, g(\mathbf{X}). \tag{3}$$

with $\mathbf{X}$ as the unique configuration of random variables describing the defect, $g(\mathbf{X})$ their joint probability density function, and N the number of traps. For oxide defects close to the interface we obtain the charge contribution $Q_{\mathrm{ox}}(t) = \mathrm{q}\langle f_2(t)\rangle$.

Although the analytic solution of (1) and (2) for a single defect is in principle straight-forward, no closed-form solution of the multiple integration in (3) is possible and approximations are necessary. Note that the transitions between state 2 and 3 are much faster than the transitions between state 1 to 2 and 3 to 1, as the former require significant structural relaxation. In other words, the charge state of the switching trap, once created, quickly follows the position of the Fermi-level. The effective model is given in Fig. 2

Consequently, (1) and (2) can be simplified to an effective rate equation (see Fig. 2)

$$\dot{f}_{\mathrm{A}} = -\, f_{\mathrm{A}} k_{\mathrm{AB}} + (1 - f_{\mathrm{A}}) k_{\mathrm{BA}}. \tag{4}$$

The probability of having positively charged defects is then

$$f_2(t) = f_{\mathrm{B}}^{+}(t) = (1 - f_{\mathrm{A}}(t)) \frac{k_{32}}{k_{23} + k_{32}}. \tag{5}$$

The solution of this equation system involves the very simple exponential transition $\exp(-t/(k_{\mathrm{AB}}+k_{\mathrm{BA}}))$, which can be approximated by a step-function, see Fig. 3. Integration over these step-functions following (3) is now in principle trivial. However, great care has to be taken to properly account for the (time and bias-dependent) boundary values of the various integrals, making the procedure extremely laborious.

In order to demonstrate how we calculated the boundary values of integration by approximating exponentials as step functions, for simplicity, we consider integration with respect to one random variable over a function $\exp(-t/(k_{\mathrm{AB}}+k_{\mathrm{BA}}))$. Let us consider, for example, X = $f(a, b, c, d)$, where a, b, c and d are random variables describing the defect. Since the rates k_{AB} and k_{BA} are functions of these random variables, the function $\exp(-t/(k_{\mathrm{AB}}+k_{\mathrm{BA}}))$ can be rewritten as $\exp(-tX)$. While integrating this function with respect to random variable 'a', $\exp(-tX)$ can be split as $\exp(-tf(a)).\exp(-tY)$ where Y = $f(b, c, d)$. Now the integration boundaries are determined by the switching function as

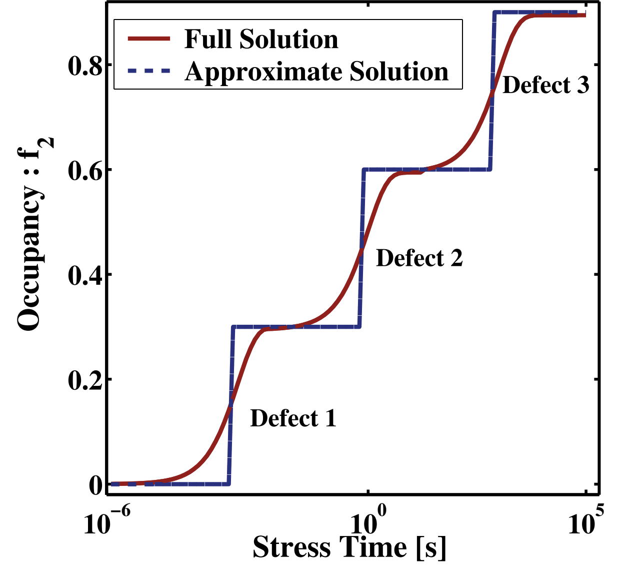

Fig. 3. Schematic of full solution and approximate solution of three defects obtained using effective rate equation is shown in Fig. 2.

$$\exp(-tX) = \begin{cases} 0 & a < a_{switch} \\ \exp(-tY) & \text{otherwise} \end{cases} \tag{6}$$

where $a_{switch} = \exp(\epsilon\; t\; f(a))$ and ϵ has a value between 2 and 3.

Using an analogous procedure, the result obtained after multiple integration using (3) is:

$$\Delta Q_{\mathrm{ox}}(t) = \frac{\mathrm{q}\Theta(S_1, f_{2\mathrm{a}}(t), f_{2\mathrm{b}}(t))}{(a_1 - a_0)(A_1 - A_0)(B_1 - B_0)} \tag{7}$$

$$f_{2\mathrm{a}}(t) = B_{\mathrm{K}} - \Theta(S_2, 0, B_{\mathrm{A}}(t)) - \Theta(S_3, 0, B_{\mathrm{Z}}(t))$$

$$f_{2\mathrm{b}}(t) = B_{\mathrm{K}} - B_{\mathrm{S}}(t)$$

where the switching function $\Theta(S, a, b)$ can be written as

$$\Theta(S, a, b) = \begin{cases} a & S \geq \log(t) \\ b & S < \log(t) \end{cases} \tag{8}$$

and other auxiliary quantities are given in Appendix. The threshold voltage shift due to a change in oxide charge is given by $\Delta V_{\mathrm{th}}^{\mathrm{ox}}(t) = -\Delta Q_{\mathrm{ox}}(t)/C_{\mathrm{ox}}$.

III. Simplified Solution

Although very accurate, (7) is obviously unsatisfactory from an engineering point of view. It has been reported that for short stress times the initial degradation follows a logarithmic dependence of stress time [3, 6, 10, 14]. Thus, in the most important region after the onset of degradation t_0 and prior to saturation, a good analytic approximation of (7) is obtained by a Taylor expansion on a logarithmic time scale

$$\Delta Q_{\mathrm{ox}}(t) = B(F, T) \log_{10}(t/t_0) \tag{9}$$

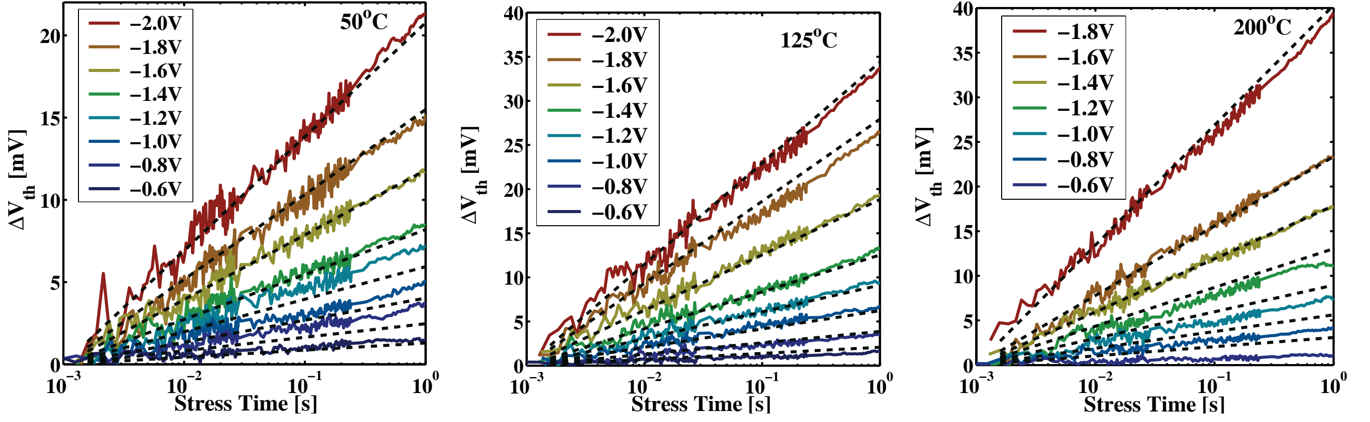

Fig. 4. Comparison of the analytic solution (dotted lines) with short-time experimental data recorded in the wide range $V_\mathrm{G} = -0.6\ldots-2.0\,\mathrm{V}$ (solid lines). The only free parameters of the model are easily extracted from this dataset to be $D = 7$ and $F_\mathrm{c} = 2\,\mathrm{MV/cm}$. The values of the hole concentrations p_s and p_r and the electric field F are obtained from a simple Poisson solver calibrated to an experimental CV curve but may be replaced by standard compact modeling expressions.

with the prefactor $B(F,T)$ as

$$B(F,T) = D\,(k_\mathrm{B}T)^2\left[\frac{F^2}{{F_\mathrm{c}}^2} + 2\log\left(\frac{p_\mathrm{s}}{p_\mathrm{r}}\right)\right] \tag{10}$$

and

$$D = \frac{E_\mathrm{B}^\mathrm{m} - E_\mathrm{A}^\mathrm{m} + E_{\mathrm{T}'}^\mathrm{m} - E_\mathrm{T}^\mathrm{m} + \sigma_\mathrm{B} + \sigma_\mathrm{A} - \sigma_\mathrm{T} - \sigma_{\mathrm{T}'}}{\sigma_\mathrm{T}\sigma_\mathrm{A}\sigma_\mathrm{B}}.$$

E_A^m and σ_A are the mean and the half-width of the uniform distribution of the activation energy required for transition between 1 and 2, E_B^m and σ_B describe the activation energy required for the transition between 3 and 1, E_T the trap precursor level, $E_{\mathrm{T}'}$ the switching trap level, σ_T and $\sigma_{\mathrm{T}'}$ the half width of the distributions of the trap precursor level and the switching trap level respectively, F_c the multiphonon-field-emission reference field, and p_s and p_r the surface hole concentration during stress and pre-stress, respectively. For low stress fields (operating conditions), the bias-dependence of the prefactor $B(F,T)$ is given by the weak $\log(p_\mathrm{s}/p_\mathrm{r})$ term, while for the high-field stress the $(F/F_\mathrm{c})^2$ term begins to dominate. The temperature dependence is given by T^2 and can be fit in our experimental window by an Arrhenius law with activation energy of about $100\,\mathrm{mV}$ which is the typically observed activation energy of NBTI.

The onset of degradation t_0 depends on F and T but is for standard NBTI measurements much smaller than the measurement resolution t_M. Thus, in on-the-fly (OTF) measurements a dependence of $\Delta Q_\mathrm{ox}^{OTF} = B\log_{10}(t/t_\mathrm{M})$ is observed. The $\Delta Q_\mathrm{ox}^{OTF}$ is calculated by subtracting $\Delta Q_\mathrm{ox}(t_M)$ from $\Delta Q_\mathrm{ox}(t)$.

IV. Validation of the Model

In Fig. 4 the experimental bias-dependence of $\Delta V_\mathrm{th}^\mathrm{ox}(t)$ at three temperatures is compared to (9) where excellent agreement is ob-

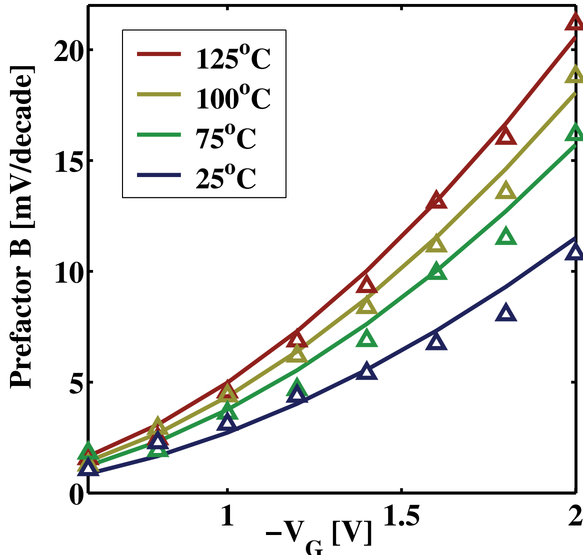

Fig. 5. Comparison of $B(F,T)$ obtained using (10) (solid lines) as a function of gate bias against the values extracted from measured data [8] (symbols) for four different temperatures.

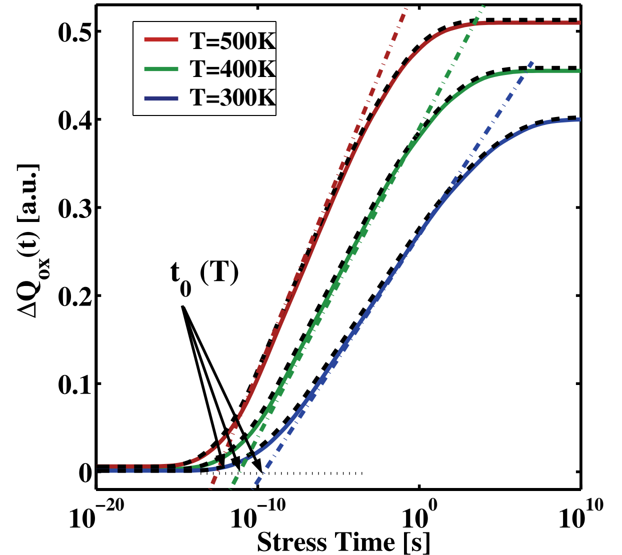

Fig. 6. Comparison of the simulated $\Delta V_\mathrm{th}(t)$ for different temperature at a bias of -1.8V. Shown is the numerical solution (solid lines), the full analytic solution (7) (dashed lines), and the simplified analytic expression (9) (dashed-dotted lines). The arrows indicate the temperature-dependent onset of degradation t_0.

tained in the full temperature and bias range using only two parameters D and F_c. However, no details on the distribution of the defect properties can be extracted from OTF measurements alone (e.g. E_T, E_B, σ_A, etc.) as they are all lumped into D. Fig. 5 shows $B(F,T)$ obtained using (10) against experimental data as a function of gate bias at different temperatures.

Fig. 6 shows a comparison of the full and simplified analytic expressions against the numerical data. The degradation starts at t_0 and the initial degradation follows a logarithmic time-dependence and finally saturates. The full analytic solution matches well with numerical simulation. The simplified model gives the degradation of logarithmic time-dependence regime as shown in Fig. 6.

Another important result is the onset of degradation, approximately given by t_0. Fig. 6 and Fig. 7 demonstrate that at the usual NBTI conditions t_0 is outside the measurement range for this device. At lower temperatures, however, t_0 can be made visible [15].

V. Conclusions

In this paper, we presented an analytical model for the recoverable component of NBTI. A simplified model which is valid in the logarithmic time-dependent regime is also presented. This model gives insight into the temperature and field dependence of threshold voltage shift due to NBTI. The results from the model are validated for different temperature and bias conditions. Finally, the dependence of temperature and field on the onset of degradation t_0 are also investigated in this paper.

VI. Appendix

Additional auxiliary functions for the full analytic solution (7) are given below:

$$
\begin{aligned}
B_K &= -(B_1 - B_0)\left[(B_1 + B_0)^2 + 3(a_1 - A_0)\right.\\
&\qquad\left.(B_1 + B_0) - C_{f1}\right]/6,\\
B_i(t) &= (B^i_{f1} - B^i_{f2})\left[(B^i_{f1} + B^i_{f2})C_B + C^i_{f2}\right]/2,\\
C_{f1} &= B_{f1}B_1 + 3C_1 + 3C_B\left[2(a_1 - a_0) - C_B\right],\\
B^{\mathrm{A}}_{f1} &= C_B - a_1 - a_f, \qquad B^{\mathrm{A}}_{f2} = B_0,\\
C^{\mathrm{A}}_{f2} &= a_1(a_1 - 2a_f) - A_0(A_0 - 2a_f) - {a_0}^2\,(1 - 2C_B/a_0),\\
B^{\mathrm{Z}}_{f1} &= a_f - a_0, \qquad B^{\mathrm{Z}}_{f2} = C_B - a_1 - a_f,\\
C^{\mathrm{Z}}_{f2} &= (a_f - A_0)(A_0 - 2a_1) + 2C_B(a_1 - a_f) - {C_B}^2)\\
B^{\mathrm{S}}_{f1} &= B_1, \qquad B^{\mathrm{S}}_{f2} = -a_f,\\
C^{\mathrm{S}}_{f2} &= a_1 a_f^2(a_1 - 2a_f)(1 - 2C_B/a_1),\\
a_f &= \log(20tk_s/9) + (F_{\mathrm{s}}/F_{\mathrm{c}})^2,\\
C_B &= -(F_{\mathrm{r}}/F_{\mathrm{c}})^2 + (F_{\mathrm{s}}/F_{\mathrm{c}})^2 - \log(\nu/k_s),\\
S_1 &= A_0 - \log\left((20/9)\nu\right), \qquad S_2 = B_0 - a_f - C_B + a_0,\\
S_3 &= B_0 - a_f + a_0, \qquad k_s = p_{\mathrm{s}}v^{\mathrm{th}}\sigma_{\mathrm{p}}\\
a_0 &= \beta(E_V - E^m_T + \sigma_T) \qquad a_1 = \beta(E_V - E^m_T - \sigma_T)\\
b_0 &= \beta(E^m_{T'} - \sigma_{T'} - E_V) \qquad b_1 = \beta(E^m_{T'} + \sigma_{T'} - E_V)\\
A_0 &= \beta(E^m_A - \sigma_A) \qquad A_1 = \beta(E^m_A + \sigma_A)\\
B_0 &= \beta(E^m_B - \sigma_B) \qquad B_1 = \beta(E^m_B + \sigma_B)
\end{aligned}
$$

where F_{s} and F_{r} are the stress and pre-stress electric fields and other parameters are like in [8].

VII. Acknowledgements

This research work has received funding from the European Community's Seventh Framework Programme under Grant Agreement No. 216436 (project ATHENIS).

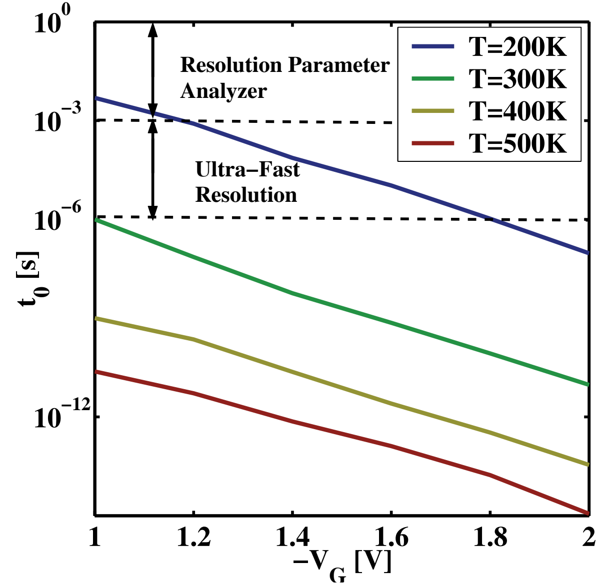

Fig. 7. The temperature and bias dependence of the onset of degradation t_0. Above room temperature, only at low bias ($V_{\mathrm{G}} \sim -1\,\mathrm{V}$) t_0 may be experimentally observed using an ultra-fast setup.

References

[1] K.O. Jeppson and C.M. Svensson, "Negative Bias Stress of MOS Devices at High Electric Fields and Degradation of MNOS Devices," *JAP*, vol. 48, no. 5, pp. 2004–2014, 1977.

[2] M.A. Alam, "A Critical Examination of the Mechanics of Dynamic NBTI for pMOSFETs," in *IEDM*, 2003, pp. 345–348.

[3] H. Reisinger, O. Blank, W. Heinrigs, A. Mühlhoff, W. Gustin, and C. Schlünder, "Analysis of NBTI Degradation- and Recovery-Behavior Based on Ultra Fast V_{th}-Measurements," in *IRPS*, 2006, pp. 448–453.

[4] C. Shen, M.-F. Li, C. E. Foo, T. Yang, D.M. Huang, A. Yap, G.S. Samudra, and Y.-C. Yeo, "Characterization and Physical Origin of Fast V_{th} Transient in NBTI of pMOSFETs with SiON Dielectric," in *IEDM*, 2006, pp. 333–336.

[5] T. Grasser, B. Kaczer, Ph. Hehenberger, W. Goes, R. O'Connor, H. Reisinger, W. Gustin, and C. Schlünder, "Simultaneous Extraction of Recoverable and Permanent Components Contributing to Bias-Temperature Instability," in *IEDM*, 2007, pp. 801–804.

[6] T. Grasser, "Negative Bias Temperature Instability: Modeling Challenges and Perspectives," in *IRPS*, 2008, (Tutorial).

[7] D.K. Schroder, "Negative Bias Temperature Instability: What Do We Understand?," *MR*, vol. 47, no. 6, pp. 841–852, 2007.

[8] T. Grasser, B. Kaczer, W. Goes, Th. Aichinger, Ph. Hehenberger, and M. Nelhiebel, "A Two-Stage Model for Negative Bias Temperature Instability," in *IRPS*, 2009, pp. 33–44.

[9] A.J. Lelis and T.R. Oldham, "Time Dependence of Switching Oxide Traps," *T-NS*, vol. 41, no. 6, pp. 1835–1843, Dec 1994.

[10] V. Huard, C. Parthasarathy, N. Rallet, C. Guerin, M. Mammase, D. Barge, and C. Ouvrard, "New Characterization and Modeling Approach for NBTI Degradation from Transistor to Product Level," in *IEDM*, 2007, pp. 797–800.

[11] M.J. Kirton and M.J. Uren, "Noise in Solid-State Microstructures: A New Perspective on Individual Defects, Interface States and Low-Frequency (1/f) Noise," *Adv.Phys.*, vol. 38, no. 4, pp. 367–486, 1989.

[12] S. Makram-Ebeid and M. Lannoo, "Quantum Model for Phonon-Assisted Tunnel Ionization of Deep Levels in a Semiconductor," *PRB*, vol. 25, no. 10, pp. 6406–6424, 1982.

[13] S.D. Ganichev, W. Prettl, and I.N. Yassievich, "Deep Impurity-Center Ionization by Far-Infrared Radiation," *Phys.Solid State*, vol. 39, no. 1, pp. 1703–1726, 1997.

[14] T. Grasser, B. Kaczer, Th. Aichinger, W. Goes, and Michael Nelhiebel, "Defect Creation Stimulated by Thermally Activated Hole Trapping as the Driving Force Behind Negative Bias Temperature Instability in SiO_2, SiON, and High-k Gate Stacks," in *IIRW*, 2008.

[15] R. Southwick, B. Knowlton, B. Kaczer, and T. Grasser, "On the Thermal Activation of Negative Bias Temperature Instability," in *IIRW*, 2009.

Questions and Answers

Q1: Can you explain high-k PBTI and NBTI in the same model?

A1: We have not directly tried this, but expect some similarities in the physical processes between NBTI in SiON pMOS and PBTI on HK nMOS devices due to the similar recovery trends observed in both technologies.